Received: 1 March 2020 | Revised: 21 June 2020 | Accepted: 24 July 2020

DOI: 10.1002/ijc.33252

MOLECULAR CANCER BIOLOGY

IJC International Journal of Cancer

The aryl hydrocarbon receptor promotes inflammation-induced dedifferentiation and systemic metastatic spread of melanoma cells

Miriam Mengoni | Andreas Dominik Braun | Evelyn Gaffal | Thomas Tüting

Laboratory for Experimental Dermatology, Department of Dermatology, University Hospital Magdeburg, Magdeburg, Germany

Correspondence
Thomas Tüting, Laboratory for Experimental Dermatology, Department of Dermatology, University Hospital Magdeburg, Leipziger Straße 44, 39120 Magdeburg, Germany.
Email: thomas.tueting@med.ovgu.de

Funding information
Deutsche Forschungsgemeinschaft, Grant/Award Number: SFB 854 Project A27; Else Kröner-Fresenius-Stiftung, Grant/Award Numbers: Bonn NeuroImmunology (BonnNI) program, 2017_Kolleg.07; TP3, 2017_Kolleg.07; TP4

Abstract

The aryl hydrocarbon receptor (AHR) is a ligand binding-transcription factor of the basic helix-loop-helix family regulating multiple cellular functions such as differentiation, cell cycle, apoptosis, and inflammatory reactions. In neoplastic diseases, the AHR has been described to modulate proliferation and differentiation in dichotomous ways, either inhibiting or augmenting the growth of tumors. The precise role of AHR in melanoma is mostly unknown. Here, we report a functional effect of AHR activation on inflammation-induced melanoma cell dedifferentiation and the development of lung metastases in a mouse model. Via in silico analyses of "The Cancer Genome Atlas" human melanoma cohort, we detected a correlation between AHR expression levels and a dedifferentiated melanoma cell phenotype with an invasive gene signature, which we were able to functionally recapitulate in a panel of human melanoma cell lines. Both human and mouse melanoma cell lines upregulated AHR expression after inflammatory stimulation with tumor necrosis factor-α (TNF-α). Activation of AHR in human and mouse melanoma cell lines with the endogenous ligand formylindolo(3,2-b)carbazole (FICZ) promoted inflammation-induced dedifferentiation in vitro. Importantly, mouse melanoma cells with CRISPR/Cas9-mediated disruption of the AHR gene showed impaired in vivo tumor growth after transplantation in the skin as well as decreased numbers of spontaneous lung metastases. Taken together, our results demonstrate a functional role for AHR expression in melanoma development and metastatic progression. This provides a scientific basis for future experiments that further dissect the underlying molecular mechanisms and assess the potential for AHR inhibition as part of multimodal melanoma treatment strategies.

KEYWORDS

aryl hydrocarbon receptor, differentiation, inflammation, melanoma, metastasis

Abbreviations: AHR, aryl hydrocarbon receptor; CCLE, Cancer Cell Line Encyclopedia; FICZ, formylindolo(3,2-b)carbazole; GO-BP, Gene Ontology Biological Process; IDO, indoleamine 2,3-dioxygenase; LPS, lipopolysaccharide; NGFR, nerve growth factor receptor; TCGA, The Cancer Genome Atlas ; TNF-α, tumor necrosis factor-α.

1 | INTRODUCTION

Despite increasing efforts for preventive and therapeutic options, the incidence of cutaneous melanoma continues to increase in European countries and the United States. This trend is projected to uphold in the near future.[1] The major environmental risk factor for melanoma development is UV light exposure. UV irradiation can induce oncogenic mutations and at the same time can promote an inflammatory microenvironment that supports the survival, proliferation, and migration of genetically altered melanocytes.[2-5] Proinflammatory mediators such as tumor necrosis factor-α (TNF-α) can promote the emergence of dedifferentiated melanoma cell phenotypes that are thought to reactivate the migratory potential of their embryonal precursors in the neural crest.[6]

UV irradiation also generates the tryptophan derivative formylindolo (3,2-b)carbazole (FICZ) in the skin which is a high-affinity ligand for the aryl hydrocarbon receptor (AHR). The AHR is a transcription factor of the basic helix-loop-helix Per-Arnt-Sim family that was initially described in xenobiotic metabolism and is highly expressed in barrier organs like the skin.[7-11] First observations linking AHR activation with pigmentation and melanocyte biology derive from accidental mass-poisoning incidents, for example, in Taiwan or Japan.[12,13] In support of this connection, it was found that mice lacking the AHR gene show impaired skin tanning.[14] Large-scale gene expression analyses in the Cancer Cell Line Encyclopedia (CCLE) revealed that melanoma cell lines can also express AHR.[15] Furthermore, shRNA-mediated knockdown of AHR led to growth inhibition, providing first evidence for a functional role of AHR.[16] The link between AHR and melanoma was further strengthened by recent genome-wide association studies that implicate the AHR gene locus with increased risk to develop cutaneous melanoma.[17,18]

In our work, we further explored a potential function of AHR signaling in melanoma pathogenesis. We show that the expression of AHR is enhanced by inflammatory mediators and augments inflammation-induced dedifferentiation in human and mouse melanoma cells. Moreover, we observe that the AHR expression promotes metastatic tumor progression in a syngeneic mouse model in vivo.

What's New?

The aryl hydrocarbon receptor (AHR) has important functions in mediating xenobiotic metabolism and in regulating numerous enzymes and transcriptional programs in cells. AHR also is expressed in melanoma and its knockdown has been shown to inhibit tumor cell growth. In our study, the AHR was found to promote inflammation-induced dedifferentiation of both human and mouse melanoma cells in vitro. In syngeneic immunocompetent mice, AHR expression promoted metastatic dissemination of transplanted melanoma cells. The findings support emerging evidence that the AHR functionally participates in melanoma pathogenesis and provide a rationale to further investigate the AHR as a putative therapeutic target.

2 | MATERIALS AND METHODS

2.1 | Cell culture

Human MZ7 melanoma cells (or MZ-MEL-7, RRID: CVCL_1436) were provided by T. Wölfel (Mainz, Germany) in 2010. The MaMel cell lines were established by D. Schadendorf (Essen, Germany) and provided to our laboratory between 2012 and 2013 (Ma-Mel-19 RRID: CVCL_A156, Ma-Mel-54a RRID: CVCL_A189, Ma-Mel-65 RRID: CVCL_A200, Ma-Mel-71 RRID: CVCL_A207, Ma-Mel-102 RRID: CVCL_A126). All human melanoma cell lines used in our study were authenticated using STR profiling in 2020 (Microsynth, Balgach, Switzerland). HCmel cell lines were derived from Hgf-Cdk4^{R24C} mice as described previously.[5,19] Monoclonal HCmel12 AHR knockout variants (HCmel12 AHR KO) were generated using the CRISPR-Cas9 genome engineering technology. All HCmel cell lines were cultured in RPMI 1640 medium (Life Technologies, Carlsbad, CA) supplemented with 20% fetal bovine serum (Biochrome, Berlin, Germany), 2 mM L-glutamine, 10 mM non-essential amino acids, 1 mM HEPES, 100 U/mL penicillin and 100 μg/mL streptomycin (all from Life Technologies) and 20 μM 2-mercaptoethanol (Sigma, St. Louis, MO) in a humidified incubator with 5% CO_2 at 37°C. RPMI 1640 medium supplemented with 10% FCS and the previously described supplements served as a culture medium for all human melanoma cell lines used in our study. For cytokine stimulations, cells were treated with 1000 U/mL recombinant TNF-α (mouse or human, both Peprotech, Rocky Hill, NJ) and/or 1 μM FICZ (Enzo, Farmingdale, NY) dissolved in DMSO (Sigma). Vehicle controls were performed with DMSO in a final concentration of 0.1%. For the retrovirus production, HEK293T (RRID: CVCL_0063) cells, obtained from ATCC, were maintained in DMEM medium (Life Technologies) containing the same supplements. Cells were freshly thawed every 2 months. All cell lines used in our study were routinely tested for mycoplasma contamination via PCR monthly. All experiments were performed with mycoplasma-free cells.

2.2 | Cloning of AHR-sgRNA CRISPR-Cas9 plasmid

pX330-U6-Chimeric_BB-CBhhSpCas9 (pX330) (Addgene plasmid #42230) was digested with FastDigest BpiI (Thermo Fisher Scientific, Waltham, MA) and purified via agarose gel electrophoresis. DNA oligonucleotides encoding for AHR sgRNAs (Microsynth) were cloned into the digested pX330 vector. Sequences of DNA oligos are listed in Supplementary Table 1.

2.3 | Generation of genetically AHR-deficient HCmel12 cells

To generate genetically AHR-deficient HCmel12 melanoma cells, 5×10^5 HCmel12 cells were seeded into 12-well plates 1 day before

transfection. Subsequently, the cells were transfected with 1.6 μg AHR-sgRNA plasmid and 0.4 μg pRP-TagGFP2 in Opti-MEM medium (Thermo Fisher Scientific) supplemented with Fugene HD transfection reagent (Promega, Fitchburg, WI) according to the manufacturer's protocol. An AHR-competent, HCmel12 CRISPR control cell line (hereafter referred to as HCmel12 CRISPR ctrl cells) were obtained after transfection with 1.6 μg of "empty" CRISPR vector and 0.4 μg pRP-TagGFP2 plasmid. After 48 hours, GFP-positive cells were sorted with a FACSAria II Cell Sorter (BD Biosciences, San Jose, CA) and single-cell cloned via limiting dilution. Genetic loss of AHR was validated by next generation sequencing on a MiSeq Sequencer (Illumina, San Diego, CA) and after analysis using the Outknocker tool (http://www.outknocker.org).

2.4 | Retroviral gene transfer

pRP-TagGFP2 was generated by subcloning of TagGFP2-cDNA into the pRP vector using the BamHI and NotI restriction sites. HEK 293T cells were transfected with the retroviral helper plasmids (gag-pol [Addgene plasmid #14888] and pCMV VSV-G [Addgene plasmid #14887], kindly provided by E. Latz, Bonn, Germany) and pRP-TagGFP2 by calcium phosphate transfection according to standard protocols. Retrovirus containing supernatant was filtered using a 0.45 μM pore size syringe filter and added to target cells. Selection with 10 μg/mL puromycin (AppliChem, Darmstadt, Germany) was started 48 hours after transduction for 5 days.

2.5 | Cell growth assay

Cell growth was quantified by counting viable cells using Trypan blue. In short, genetically manipulated HCmel12 cells and HCmel12 control cells (transfected with an "empty" CRISPR vector) were seeded at low density in biological triplicates and incubated at standard conditions for 72 hours. After this time, all cells were harvested and collected following standard protocols. Cell number was determined using a hemocytometer with a DME microscope (Leica, Wetzlar, Germany).

2.6 | Transwell migration assay

Migration of fluorescently labeled HCmel12 cells was quantified using a Boyden Chamber assay. Briefly, TagGFP2-positive HCmel12 melanoma cells were treated with 1000 U/mL recombinant TNF-α for 72 hours. Untreated cohorts served as control. From these, 2×10^4 melanoma cells in were resuspended in RPMI 1640 medium supplemented with 1% FCS and placed in the upper chamber of uncoated PET filters (8 μm pore size, Corning, Corning, NY) and subsequently incubated at 37°C/5% CO2 to adhere. To assess the directed migration after a FCS gradient, the lower chamber was filled with RPMI 1640 medium supplemented with 10% FCS. After incubation for 16 hours, transmigrated cells on the lower surface of the membrane were fixed with 4% paraformaldehyde (Carl Roth, Karlsruhe, Germany). Three representative high power fields were counted using a DM IRB microscope (Leica). The experiment was performed in triplicate and repeated independently at least three times.

2.7 | Immunoblot analysis

Whole cell lysates were extracted from cultured cells using the M-PER mammalian protein reagent supplemented with protease and phosphatase inhibitors (all Thermo Fisher Scientific) according to the manufacturer's protocol. Protein concentrations were quantified with a Pierce BCA Protein Assay Kit (Thermo Fisher Scientific) at 562 nm in a microplate reader (Tecan Group, Männedorf, Switzerland). Samples were prepared containing 10 μg protein, Roti-Load (Roth) and nuclease-free water and denatured at 95°C prior to loading. In a next step, samples were separated via 10% SDS-PAGE and transferred to a 0.45 μM polyvinylidene difluoride membrane (GE Healthcare, Boston, MA) by wet blotting (BioRad, Hercules, CA). After blocking with 5% milk (Roth), blots were immunostained at 4°C overnight. Bound antibodies were detected with horseradish peroxidase (HRP)-conjugated secondary antibodies and the SignalFire ECL Reagent (Cell Signaling, Danvers, MA) according to the manufacturer's instructions. Chemiluminescence was visualized using an Octoplus QPLEX-Imager (NH DyeAGNOSTICS, Halle, Germany). Used antibodies were as follows: sheep anti-mouse AHR polyclonal antibody (R&D, Minneapolis, MI, AF6697), sheep anti-human AHR polyclonal antibody (R&D, AF6185), mouse β-Actin monoclonal antibody (Santa Cruz, Dallas, TX, sc-47 778), goat anti-mouse nerve growth factor receptor (NGFR) polyclonal antibody (R&D, AF1157) goat anti-mouse/human gp100 polyclonal antibody (Abcam, Cambridge, UK, ab52058), rabbit anti-mouse/human/rat TYRP1 polyclonal antibody (Novus, Centennial, CO, NBP1-88370), rabbit anti-mouse/human TRP2 polyclonal antibody (Abcam, ab74073), goat anti-rabbit IgG HRP-linked antibody (Cell Signaling, #7074S), mouse anti-goat IgG HRP linked antibody (Santa Cruz, sc-2354) and donkey anti-sheep IgG HRP-linked antibody (R&D, HAF016).

2.8 | Quantitative real-time PCR

Total RNA from cultured cells was isolated and purified using the NucleoSpin RNA XS kit (Macherey-Nagel, Düren, Germany). RNA concentration was quantified with a NanoQuant Plate using a Spark 10 M multimode microplate reader (Tecan Group). Complementary DNA was synthesized with the GoScript reverse transcription system and oligo(dT)15 primers (both Promega) according to the manufacturer's protocol. Real-time quantitative PCR analysis was performed with the GoTaq qPCR Master Mix (Promega) on a peqSTAR 96Q-thermocycler (PEQLAB Biotechnology, Erlangen, Germany). All qRT-PCR reactions were prepared in technical duplicates or triplicates in a total volume of 20 μL. The sequences of primers (Microsynth) are given in Supplementary Table 1. Relative expression to the reference gene ubiquitin was calculated with the double delta Ct analysis using the following

equations: ΔCt = Ct(target gene) − Ct(reference gene); ΔΔCt = ΔCt (condition 1) − ΔCt(reference condition).

2.9 | Analysis of published datasets

Gene expression data (RNA-seq) of The Cancer Genome Atlas (TCGA) melanoma cohort (SKCM) was accessed through the cBioportal for Cancer Genomics (http://www.cbioportal.org) using the R-based package CGDS-R and following TCGA guidelines for the use of TCGA data (https://cancergenome.nih.gov/). We retrieved RSEM-normalized values for the individual gene expression values of interest and ordered according to their *AHR* expression value. Enrichment of Gene-Ontology terms was analyzed with the R-package clusterProfiler. Expression values were log2-transformed and median centered. Dataset GSE51221 was retrieved from the gene expression omnibus via the package GEOquery, CCLE gene expression data was downloaded from the CCLE data repository (https://portals.broadinstitute.org/ccle/data, data version 2019-01-02). Differential gene expression was analyzed using a Bayes-moderated t-statistic using the limma package. Moving averages were calculated with right alignment using the zoo package and window sizes of 20 for the TCGA dataset, 5 for the CCLE dataset and 3 for the GSE51221 dataset.

2.10 | Mice

Wild-type C57BL/6J mice were purchased from Janvier (Le Genest-Saint-Isle, France) or taken from own breeding. Age- and sex-matched cohorts of mice were randomly allocated to the different experimental groups at the start of each experiment.

2.11 | Tumor transplantation

Cohorts of syngeneic C57BL/6J mice were injected intracutaneously with 2×10^5 HCmel12 CRISPR ctrl cells or a mixture of three HCmel12 AHR CRISPR KO monoclones in equal proportions resuspended in 100 μL PBS (Life Technologies) into the right flank. Tumor growth was monitored by inspection and palpation. Tumor size was measured at least twice times weekly with a vernier caliper and recorded as the mean diameter of two perpendicular measurements. Mice were sacrificed when tumors exceeded 20 mm in diameter or when signs of illness were observed. Lung metastases were counted by macroscopic inspection. All experiments were performed in groups of five or more mice and repeated independently three times.

2.12 | Statistical analyses

We considered tumor growth, cell proliferation and migration as well as qRT-PCR expression as normally distributed with similar variances. For these data, we performed parametric testing with unpaired, two-sided Student's *t* tests. The pulmonary metastasis counts were tested with a nonparametric Mann-Whitney *U* test. Survival probabilities were calculated with Kaplan-Meier estimators and compared by log-rank test statistics. RNAseq expression data was corrected for multiple testing via Benjamini-Hochberg false discovery rate adjustment. The null hypothesis was rejected for $P < .05$. All statistical analyses were conducted in the R computing environment.

3 | RESULTS

3.1 | AHR is expressed in human melanoma and correlates with an dedifferentiated phenotype

Initially, we performed bioinformatical analyses of TCGA melanoma samples to assess the expression of *AHR* in human melanoma. We detected a heterogeneous expression with approximately 10% of melanoma samples showing expression levels higher than one standard deviation from the mean (Figure 1A). Differential gene expression analysis between melanoma samples with high *AHR* levels and those with low *AHR* levels revealed 2055 genes with a log2-fold change >|2| (Table S2). Grouping of genes downregulated in *AHR* high samples by Gene Ontology Biological Process (GO-BP) terms showed strong enrichment of genes involved in the cellular pigmentation machinery (Figure 1B). Further analyses of the melanoma cohort revealed that the expression of *AHR* was inversely correlated with the expression of pigmentation genes such as *PMEL* and *TYRP1* (Figure 1C). Additionally, the expression of *AHR* was inversely correlated with a gene signature that has previously been associated with a proliferative phenotype and directly correlated with a gene signature associated with an invasive phenotype (Figure 1D).[20] Incidentally, the proliferative gene set largely contains melanocytic differentiation antigens, whereas the invasive gene set includes markers of a dedifferentiated cell state. Taken together, this supports the notion that AHR may functionally participate in melanoma pathogenesis.

3.2 | Activation of AHR enhances inflammation-induced dedifferentiation in differentiated human melanoma cell lines

Next, we sought to recapitulate the association between *AHR* and a dedifferentiated, invasive phenotype also in human cell lines. For this, we performed bioinformatic analyses on gene expression data from the CCLE. Again, *AHR* was negatively correlated with the proliferative gene signature and putatively correlated with the invasive gene signature (Figure S1A,B, left panel). These findings were also reproducible in a set of melanoma cell lines established in our laboratory that was selected to reflect the mutation spectrum and differentiation phenotypes in human melanoma (Figure 2A; Figure S1A,B, right panel). From these, we selected three differentiated and three dedifferentiated cell lines based on their expression of a set of bona fide pigmentation genes for further functional analyses. We previously reported that TNF-α can shift melanoma cells towards a more dedifferentiated cell state.[5] We therefore

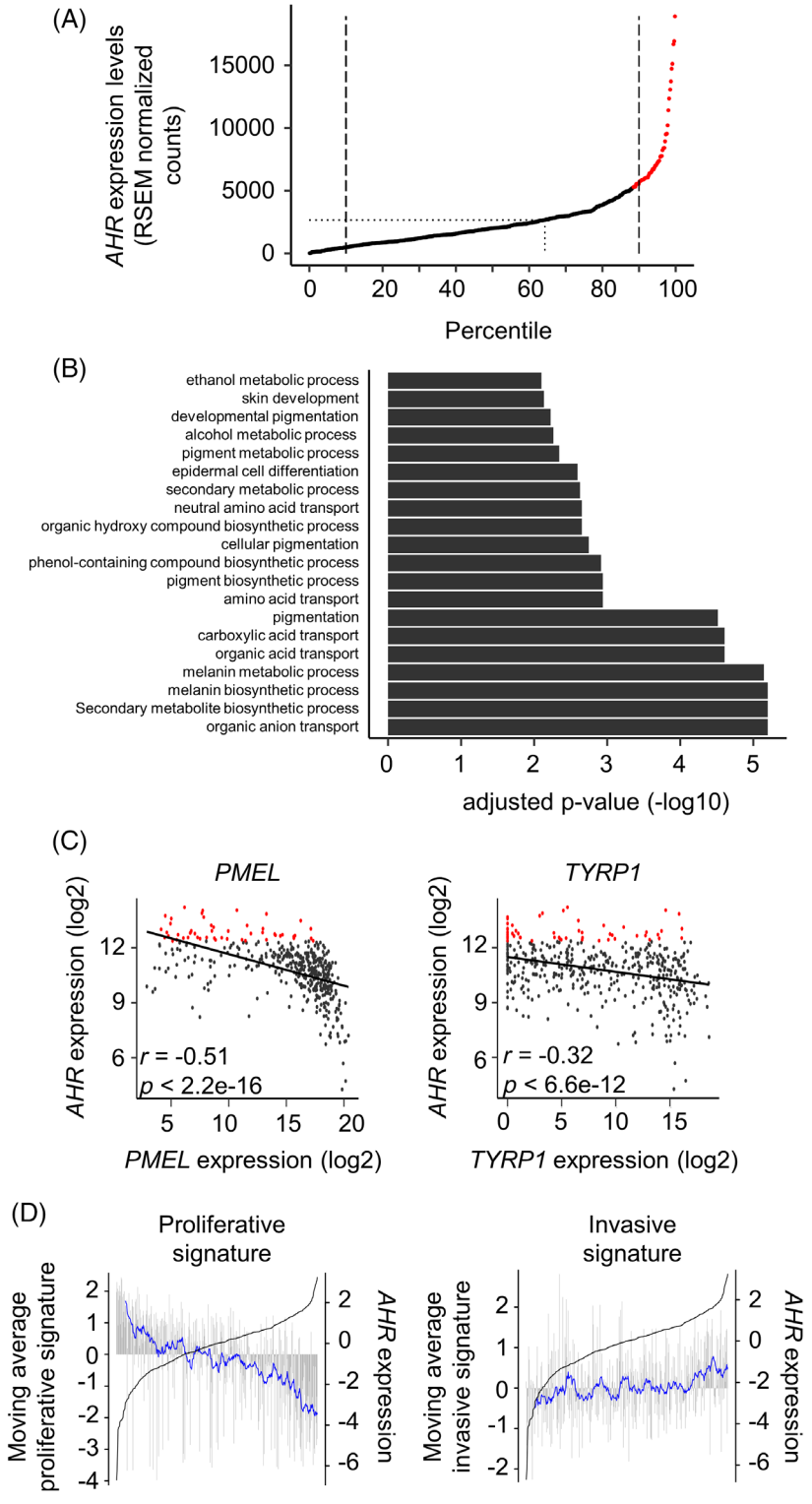

FIGURE 1 Aryl hydrocarbon receptor (AHR) expression levels correlate with a dedifferentiated melanoma phenotype in The Cancer Genome Atlas (TCGA) dataset. A, RNAseq expression levels of AHR in TCGA skin melanoma samples extracted from cBioPortal as counts normalized with the RSEM tool (n = 443). Samples are ordered by *AHR* expression. Dashed lines indicate the 10th and 90th percentiles. The dotted line marks the arithmetic mean. Samples with expression values greater than one standard deviation (SD) above the mean are marked in red. B, Enrichment of genes in Gene Ontology Biological Process (GO-BP) terms from a differential gene expression analysis between TCGA melanomas with *AHR* expression values above the 90th percentile vs those with *AHR* expression below the 10th percentile. The 20 most enriched terms are depicted. C, Correlation between AHR expression and selected markers of the differentiation status in the TCGA SKCM cohort. Regression line is shown in black. D, Moving averages between gene sets for proliferative and invasive phenotypes (2008 Hoek et al). The black line indicates the AHR expression, gray bars show individual expression values for gene sets and blue lines represent their moving average with window size 20. All values were log2-transformed prior to plotting [Color figure can be viewed at wileyonlinelibrary.com]

assessed how TNF-α treatment affects the expression of AHR and the response to AHR activation after exposure to the high-affinity AHR ligand FICZ. Interestingly, the expression of *AHR* was induced by TNF-α both in the absence and the presence of FICZ in the more differentiated melanoma cell lines but not in the dedifferentiated cell lines (Figure 2B). Strong induction of the AHR target gene *CYP1A1* could be detected after stimulation with FICZ in all cell lines regardless of TNF-α exposure (Figure 2C). Importantly, simultaneous exposure of cells to TNF-α and FICZ further decreased the mRNA levels for the melanocytic genes *MITF*, *PMEL* and *DCT* in the differentiated melanoma cell lines (Figure 2D, top row) but not in the dedifferentiated cell lines (Figure 2D, bottom row). On the protein level we also found that TNF-α leads to increased AHR expression both in the absence and the presence of FICZ in the more differentiated melanoma cell lines (Figure 2E, top lane), even

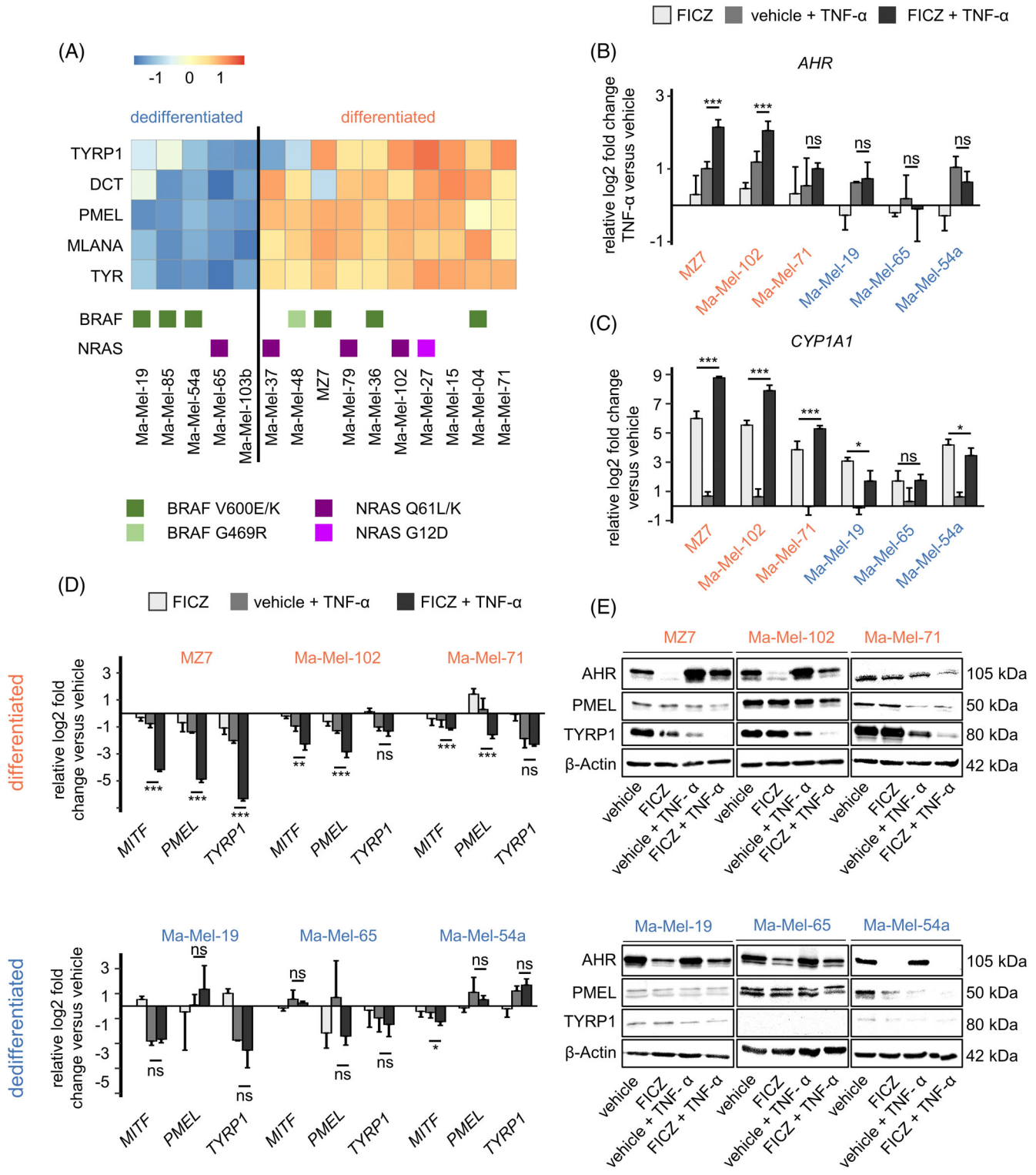

FIGURE 2 Activation of aryl hydrocarbon receptor (AHR) promotes inflammation-induced dedifferentiation in differentiated human melanoma cell lines. A, Heatmap of a human cell line panel showing z-transformed expression values for melanocytic differentiation antigens (dataset GSE51221). The mutation spectrum of cell lines for BRAF and NRAS are shown below. B-D, qRT-PCR analysis of *AHR* (B), *CYP1A1* (C) and melanocytic differentiation genes (D) for the indicated three melanocytic and three dedifferentiated human melanoma cell lines. Cells were treated for 72 hours as indicated. Shown is the relative log2-fold change (mean ± SD) when compared to vehicle-treated controls (unpaired, two-sided Student's *t* test; ns, nonsignificant; **P* < .05; ***P* < .01; ****P* < .005). *GAPDH* served as the reference gene. E, Corresponding Western blot analyses for melanoma cells treated for 72 hours as indicated. β-Actin served as a loading control. Data in B-E are representative for one out of three independently performed experiments. qRT-PCR data in B-D were performed in three biological and two technical replicates [Color figure can be viewed at wileyonlinelibrary.com]

though FICZ-dependent activation of AHR promotes posttranslational ubiquitin-mediated protein degradation regardless of TNF-α exposure (a well described phenomenon observed in all melanoma cell lines). In agreement with the mRNA analyses, we observed enhanced inflammation-induced dedifferentiation of the differentiated human melanoma cell lines after simultaneous treatment with TNF-α and FICZ when compared to TNF-α alone (Figure 2E, bottom three lanes). Together, these in vitro results demonstrate that AHR is functionally expressed in human melanoma cells and can promote the phenotypic shift towards a dedifferentiated melanoma phenotype in an inflammatory environment.

3.3 | Mouse Hgf-Cdk4^{R24C} cell lines express functional AHR

In order to study the effects of AHR in vivo, we turned to the Hgf-Cdk4^{R24C} mouse melanoma model established in our laboratory. AHR expression could be detected in the three well-characterized transplantable cell lines HCmel3, HCmel12 and HCmel31 derived from primary Hgf-Cdk4^{R24C} melanomas. AHR expression appeared to correlate inversely with the melanocytic differentiation antigens PMEL, DCT and TYRP1 and directly with expression of the NGFR (CD271), a marker associated with a dedifferentiated phenotype (Figure 3A,B). Treatment with FICZ for 24 hours resulted in strong induction of the prototypical AHR target gene *Cyp1a1* in HCmel3 and HCmel12 cells but not in HCmel31 cells (Figure 3C). These results demonstrate that functionally active AHR can be expressed in Hgf-Cdk4^{R24C} melanoma cell lines, with a putative inverse correlation between AHR expression and the melanocytic differentiation state, in agreement with the human setting.

3.4 | Inflammation induces the expression of AHR and modulates inflammatory responses in HCmel12 cells

To investigate the impact of inflammatory processes on AHR expression and signaling, we treated HCmel12 cells with combinations of TNF-α and FICZ. This resulted in a marked upregulation of AHR mRNA levels in quantitative RT-PCR analyses both in the absence and the presence of FICZ (Figure 4A). Again, strong induction of the AHR target gene *Cyp1a1* could be detected after stimulation with FICZ regardless of TNF-α exposure (Figure 4B). Because we previously observed that AHR activation promoted inflammation-induced dedifferentiation of human melanoma cells, we next assessed whether AHR activation might also have the same effect on the mouse melanoma cell line HCmel12. We found decreased mRNA levels for a panel of melanocytic differentiation genes in HCmel12 melanoma cells after treatment with TNF-α. The expression of *Pmel*, *Dct* and *Mlana* was further decreased after simultaneous exposure to FICZ (Figure 4C). The qRT-PCR results could be confirmed on the protein level as HCmel12 melanoma cells exhibited increased expression of AHR and decreased expression of the melanocytic proteins PMEL, TYRP1 and DCT in Western blot analyses (Figure 4D). Thus, similar to the human melanoma cell lines, activation of AHR signaling with FICZ promoted the inflammation-induced shift towards a more dedifferentiated state.

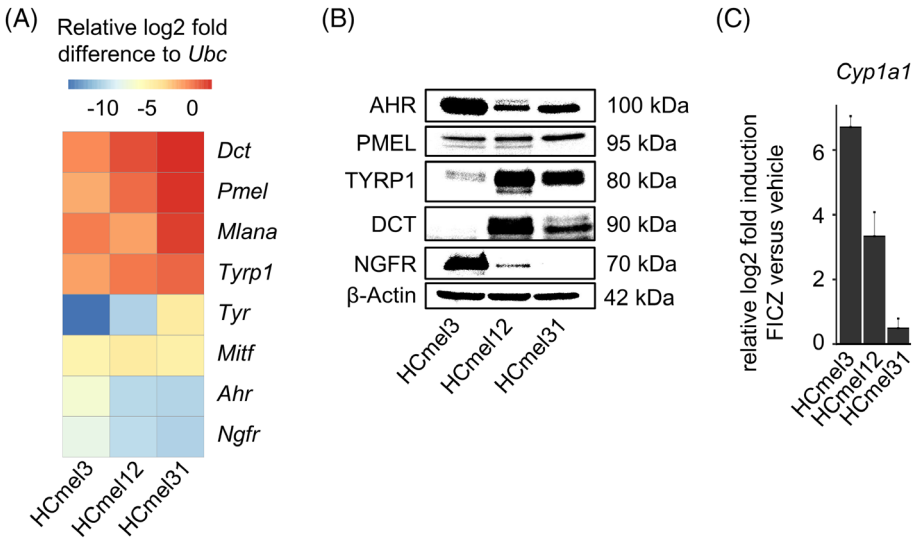

FIGURE 3 Mouse Hgf-Cdk4^{R24C} melanoma cell lines express functional aryl hydrocarbon receptor (AHR). A, mRNA abundance measured by qRT-PCR in untreated Hgf-Cdk4^{R24C} cell lines. Heatmap shows relative expression over Ubiquitin (*Ubc*). B, Western blot for AHR, nerve growth factor receptor (NGFR) and the melanocytic differentiation antigens PMEL, DCT and TYRP1 in the Hgf-Cdk4^{R24C} cell lines HCmel3, HCmel12 and HCmel31. β-Actin served as a loading control. C, qRT-PCR for *Cyp1a1*. Cells were treated with the AHR agonist FICZ or vehicle control for 24 hours. Bars indicate the relative log2-fold induction of *Cyp1a1* gene expression (mean ± SD). Data in A-C are representative for one out of three independently performed experiments. A + C were performed with three biological and three technical replicates [Color figure can be viewed at wileyonlinelibrary.com]

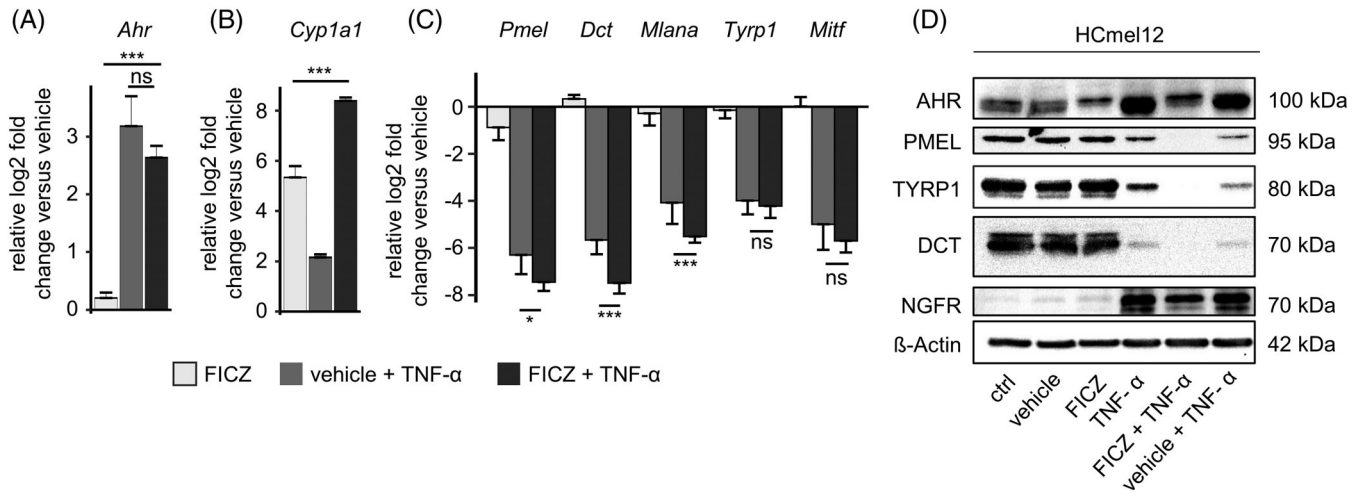

FIGURE 4 Activation of aryl hydrocarbon receptor (AHR) promotes inflammation-induced dedifferentiation in the mouse melanoma cell line HCmel12. A-C, qRT-PCR for *Ahr*, *Cyp1a1* and selected melanocytic differentiation antigens in HCmel12 cells treated as indicated for 72 hours. Shown is the relative log2-fold change (mean ± SD) when compared to vehicle-treated controls (unpaired, two-sided Student's *t* test; ns, nonsignificant; **P* < .05; ****P* < .005). D, Western blot of HCmel12 cells for melanocytic differentiation antigens. Treatments as indicated for 72 hours. Staining for DCT was performed with identical samples on a separate membrane, representative loading control shown. Data are representative for one out of three independently performed experiments. B was performed in three biological and three technical replicates

3.5 | AHR-deficient HCmel12 cells maintain a more differentiated phenotype upon inflammatory stimulation

In order to further investigate the function of AHR, we generated genetic knockouts via CRISPR/Cas9 genome editing in HCmel12 melanoma cells (Figure S2A). Successful disruption of the gene was validated via next generation sequencing and Western blot analyses (Figure S2B; Figure 5A). AHR knockout cells no longer responded to FICZ with the induction of the prototypic AHR target gene *Cyp1a1*, confirming the disruption of functional AHR signaling (Figure 5B). AHR knockout HCmel12 cells exhibited a decreased shift towards a dedifferentiated state compared to wild-type controls and failed to further dedifferentiate in response to FICZ (Figure 5C,D). This further supports a potential role for the UV-induced metabolite FICZ and the AHR signaling pathway in melanoma pathogenesis.

3.6 | Loss of AHR reduces HCmel12 melanoma growth and metastasis

Since we found that AHR expression was correlated with an expression profile associated with invasiveness in human melanomas and because AHR enhanced inflammation-induced dedifferentiation in human and mouse melanoma cell lines, we were interested to evaluate whether AHR would influence melanoma growth and metastasis in vivo. Therefore, we transplanted AHR-competent and -deficient HCmel12 melanoma cells into groups of syngeneic, immunocompetent C57BL/6J mice (Figure 6A). The median survival of mice inoculated with AHR knockout melanoma cells was slightly but significantly prolonged compared to mice inoculated with control melanoma cells (median of 30.5 vs 27 days, log-rank test *P* < .05, Figure 6B). Strikingly, AHR knockout melanomas showed an intense pigmentation in vivo (Figure 6C). Importantly, mice transplanted with AHR knockout melanoma cells revealed a significant reduction in the number and frequency of pulmonary metastases (median of 8 vs 0, Mann-Whitney *U* test *P* < .005, Figure 6D). Subsequent experiments revealed a slightly reduced proliferation rate of AHR-deficient HCmel12 cells compared to wild-type controls as well as an impaired TNF-induced migration in a transwell migration assay in vitro (Figure S3). Taken together, these results provide functional evidence that AHR expression can promote melanoma growth and metastatic disease progression.

4 | DISCUSSION

It is well established that melanoma cells can exist in a dynamic equilibrium between more differentiated cell states associated with proliferative potential and more dedifferentiated cell states associated with invasive potential and properties of their embryonal precursors from the neural crest.[20-23] Inflammatory stimuli can shift melanoma cells towards the dedifferentiated cell state.[6,19,23] In the present study, we found that AHR expression directly correlated with the degree of dedifferentiation in human melanoma samples from the TCGA cohort as well as in a panel of human and mouse melanoma cell lines. Interestingly, we also observed a direct induction of AHR after stimulation with TNF in human and mouse melanoma cell lines. A similar induction of AHR by the inflammatory mediator lipopolysaccharide (LPS) has been previously described in a mouse sepsis model.[24] As an underlying mechanism, a direct interaction of NF-kB with the AHR promoter and following upregulation after LPS as well as a direct

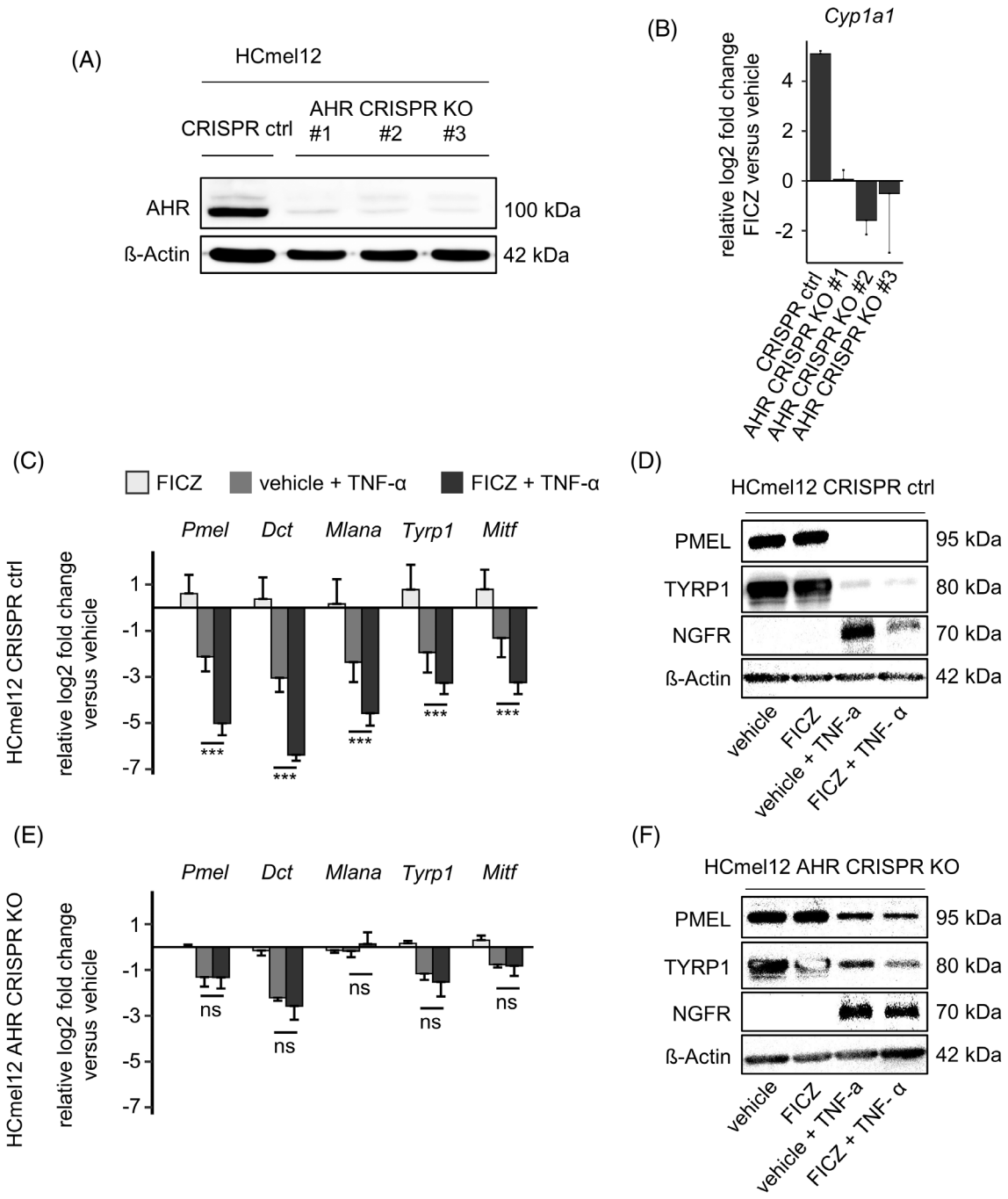

FIGURE 5 CRISPR/Cas9-mediated disruption of the aryl hydrocarbon receptor (AHR) gene in HCmel12 cells abolishes the AHR-dependent enhancement of inflammation-induced dedifferentiation. A, Western blot analysis of AHR expression comparing AHR-competent, HCmel12 CRISPR ctrl cells with HCmel12 AHR CRISPR KO cells. ß-Actin served as loading control. B, qRT-PCR for Cyp1a1 mRNA in individual HCmel12 AHR knockout clones treated with FICZ for 24 hours (mean ± SD). C, qRT-PCR comparing the expression of selected melanocytic differentiation antigens. Treatments as indicated for 72 hours. Bars represents the mean fold change compared to the housekeeping gene *Ubc* ± SD (unpaired, two-sided Student's *t* test; ns, nonsignificant; ***$P < .005$). D, Immunoblots comparing the melanoma cell differentiation states between AHR-competent, CRISPR ctrl HCmel12 cells and AHR CRISPR KO cells after 72 hours of treatment with TNF-α and/or FICZ. HCmel12 AHR CRISPR KO cells are a composite of three independent monoclones mixed in equal numbers. Data in A-D are representative for one out of three independently performed experiments. B + C were performed in three biological and three technical replicates

interaction with STAT3 with the AHR promoter has been demonstrated.[25,26] In our further analyses, we showed that activation of AHR signaling with the high-affinity ligand FICZ promotes the shift of melanoma cells towards the dedifferentiated state in an inflammatory environment, suggesting that AHR functionally participates in this process during melanoma pathogenesis. This notion is supported by our observation that AHR-deficient mouse melanoma cells show a decreased tendency for inflammation-induced dedifferentiation. The

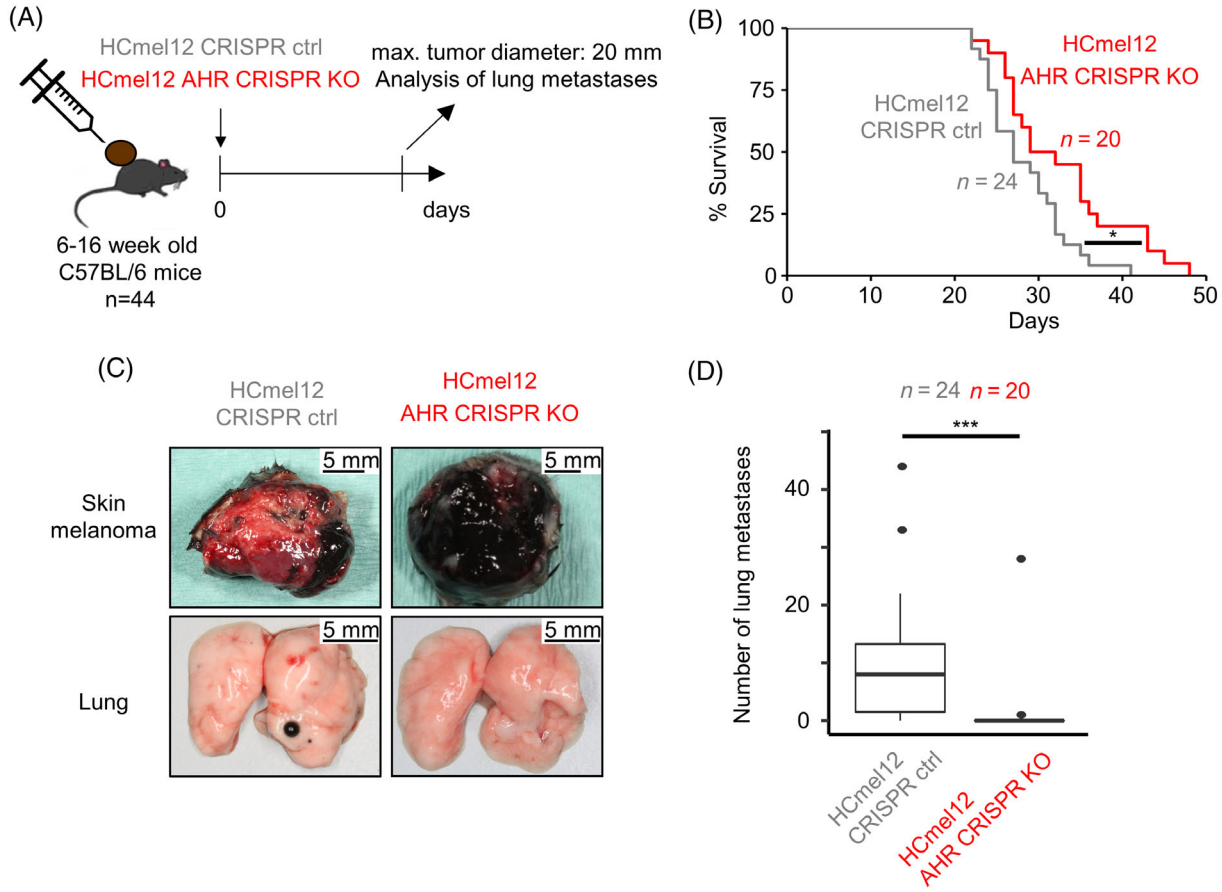

FIGURE 6 Aryl hydrocarbon receptor (AHR) gene deficient HCmel12 melanoma cells show impaired tumor growth and reduced metastatic spread in vivo. A, Experimental protocol. B, Kaplan-Meyer survival curves from mice transplanted with HCmel12 CRISPR ctrl and HCmel12 AHR CRISPR KO cells. Cumulative results of three independent experiments are shown (log-rank test; $^{*}P < .05$). C, Representative images of melanomas and lungs from both cohorts. D, Absolute quantification of pulmonary metastases in mice. Horizontal bar indicates the median, box includes the interquartile range, whiskers show 1.5× the interquartile range. Cumulative results of three independent experiments are shown (Mann-Whitney *U* test; $^{***}P < .005$). HCmel12 AHR CRISPR KO cells are a composite of three independent monoclones mixed in equal numbers [Color figure can be viewed at wileyonlinelibrary.com]

ability of AHR to promote a phenotypic switch of cancer cells toward more dedifferentiated and stem-like phenotypes has also been reported for breast cancer and oral squamous cell carcinoma.[27,28] Mechanistically, both a direct interaction of AHR with *SOX2* and an activation of *JNK* have been described.[29] Moreover, AHR has been shown to promote the expression of stemness-associated genes such as *MYC* or *KLF4* in adenocarcinoma and squamous cell carcinoma cell lines.[30] We hypothesize that in our model, the AHR signaling pathway directly influences differentiation pathways and promotes cellular plasticity of melanoma cells, allowing them to dynamically alter their phenotype and thereby enhance their malignant potential.

We observed decreased local growth and metastatic dissemination of AHR knockout melanoma cells transplanted into syngeneic immunocompetent mice. These findings support the growing body of evidence for a protumorigenic function of AHR. The AHR was first implicated in cancer pathogenesis because epidemiologic studies suggested an increased incidence of malignant tumors after prolonged exposure to toxic AHR ligands such as 2,3,7,8-tetrachlorodibenzo-*p*-dioxin as a contaminant of herbicides.[31,32] Moreover, the AHR is constitutively expressed in a broad variety of malignant tumors most likely through inflammatory signaling.[33,34] A functional role for AHR in cancer pathogenesis has been demonstrated in experiments showing that activation of AHR signaling can promote malignant transformation of epithelial cells in vitro and in vivo.[35-37] In UVB-damaged keratinocytes, AHR impairs apoptosis and thereby fosters the initiation of skin cancer.[38] In addition, AHR can promote invasive properties of various types of tumor cells including melanoma in vitro. Mechanistically, AHR activation caused a SLUG-mediated inhibition of E-cadherin expression and an increase of matrix metalloproteinases, leading to decreased cell adhesion and enhanced cell motility.[39,40] However, the role of AHR signaling in tumor progression is controversial, as pharmacologic and genetic AHR inhibition has also reported to increase tumor cell proliferation in some experimental settings including melanoma.[41] The reason for this discrepancy is currently unclear and may be explained by cell type- and cell state-dependent differences in AHR signaling.

AHR has also been implicated in the resistance of melanoma cells to signal transduction inhibitors.[42] Mechanistically, a direct binding of

the BRAF inhibitor vemurafenib as well as the MEK inhibitor PD98059 to AHR leading to its inhibition have been described.[42,43] In addition to its direct effects on tumor cells, AHR signaling can also promote an immunosuppressive microenvironment.[44] This can be mediated by the tryptophan metabolizing enzyme indoleamine 2,3-dioxygenase 1 (IDO1) which converts the amino acid tryptophan to the metabolite kynurenine that in turn can bind to and activate the AHR.[45] Kynurenine was also shown to modulate dendritic cell functions and favor the induction of regulatory T cells via AHR signaling.[46,47] More recently, it was demonstrated that activation of the IDO-Kyn-AHR axis can also confer resistance to immune checkpoint blockade.[44,48-50] Taken together, these recent observations are of clinical importance as they further support the notion that AHR not only promotes tumor progression but also therapy resistance.

In summary, our work demonstrates that AHR signaling can participate in melanoma pathogenesis and promote tumor growth and metastatic progression. Future experiments will have to address whether AHR signaling also is involved in the protumorigenic effects of UV irradiation. With the current development of IDO inhibitors and similar compounds that can modulate the IDO-Kyn-AHR axis, our model also represents a valuable tool to experimentally evaluate potential future combination therapies for melanoma, an area that is currently of intense clinical interest.

ACKNOWLEDGMENTS

We thank Susanne Bonifatius and Jeannine Herz for expert technical assistance and the UKB core facility for flow cytometry (E. Endel, P. Wurst and A. Dolf) for technical support regarding cell sorting. We also thank Naveen Shridhar for the lively discussions. Miriam Mengoni and Andreas Dominik Braun were supported by grants from the Else Kröner-Fresenius-Stiftung (Bonn NeuroImmunology [BonnNI] program, 2017_Kolleg.07; TP3, 2017_Kolleg.07; TP4). Thomas Tüting was funded by the Deutsche Forschungsgemeinschaft (SFB 854 Project A27). Open access funding enabled and organized by Projekt DEAL.

CONFLICT OF INTEREST

The authors decared no potential conflicts of interest.

ETHIC STATEMENT

All animal experiments were conducted on the C57BL/6J background according to the institutional and national guidelines for the care and use of laboratory animals with approval by the local government authorities (LANUV, NRW, Germany and LVWA, Saxony-Anhalt, Germany, approval number: 87-51.04.2010. A339).

DATA AVAILABILITY STATEMENT

The data that support the findings of this study are available from the corresponding author upon reasonable request.

ORCID

Miriam Mengoni https://orcid.org/0000-0002-1651-7114
Andreas Dominik Braun https://orcid.org/0000-0002-6954-0633
Evelyn Gaffal https://orcid.org/0000-0002-4639-9841
Thomas Tüting https://orcid.org/0000-0001-7146-0934

REFERENCES

1. Whiteman DC, Green AC, Olsen CM. The growing burden of invasive melanoma: projections of incidence rates and numbers of new cases in six susceptible populations through 2031. *J Invest Dermatol*. 2016; 136:1161-1171.
2. Tronnier M, Smolle J, Wolff HH. Ultraviolet irradiation induces acute changes in melanocytic nevi. *J Investig Dermatol*. 1995;104:475-478.
3. Chou WC, Takeo M, Rabbani P, et al. Direct migration of follicular melanocyte stem cells to the epidermis after wounding or UVB irradiation is dependent on Mc1r signaling. *Nat Med*. 2013;19:924-929.
4. Gaffal E, Landsberg J, Bald T, Sporleder A, Kohlmeyer J, Tüting T. Neonatal UVB exposure accelerates melanoma growth and enhances distant metastases in Hgf-Cdk4R24C C57BL/6 mice. *Int J Cancer*. 2011;129:285-294.
5. Bald T, Quast T, Landsberg J, et al. Ultraviolet-radiation-induced inflammation promotes angiotropism and metastasis in melanoma. *Nature*. 2014;507:109-113.
6. Riesenberg S, Groetchen A, Siddaway R, et al. MITF and c-Jun antagonism interconnects melanoma dedifferentiation with pro-inflammatory cytokine responsiveness and myeloid cell recruitment. *Nat Commun*. 2015;6:8755.
7. Rannug A, Rannug U, Rosenkranz HS, et al. Certain photooxidized derivatives of tryptophan bind with very high affinity to the Ah receptor and are likely to be endogenous signal substances. *J Biol Chem*. 1987;262:15422-15427.
8. Rannug A, Rannug U. The tryptophan derivative 6-formylindolo [3,2-b]carbazole, FICZ, a dynamic mediator of endogenous aryl hydrocarbon receptor signaling, balances cell growth and differentiation. *Crit Rev Toxicol*. 2018;48:555-574.
9. Wincent E, Amini N, Luecke S, et al. The suggested physiologic aryl hydrocarbon receptor activator and cytochrome P4501 substrate 6-formylindolo[3,2-*b*]carbazole is present in humans. *J Biol Chem*. 2009;284:2690-2696.
10. Fritsche E, Schäfer C, Calles C, et al. Lightening up the UV response by identification of the arylhydrocarbon receptor as a cytoplasmatic target for ultraviolet B radiation. *PNAS*. 2007;104:8851-8856.
11. Sadek CM, Allen-Hoffmann BL. Cytochrome P450IA1 is rapidly induced in normal human keratinocytes in the absence of xenobiotics. *J Biol Chem*. 1994;269:16067-16074.
12. Kikuchi M. Autopsy of patients with yusho. *Prog Clin Biol Res*. 1984; 137:19-30.
13. Masuda Y. Health status of Japanese and Taiwanese after exposure to contaminated rice oil. *Environ Health Perspect*. 1985;60:321-325.
14. Jux B, Kadow S, Luecke S, Rannug A, Krutmann J, Esser C. The aryl hydrocarbon receptor mediates UVB radiation-induced skin tanning. *J Invest Dermatol*. 2011;131:203-210.
15. O'Donnell EF, Koch DC, Bisson WH, Jang HS, Kolluri SK. The aryl hydrocarbon receptor mediates raloxifene-induced apoptosis in estrogen receptor-negative hepatoma and breast cancer cells. *Cell Death Dis*. 2014;5:e1038.
16. Barretina J, Caponigro G, Stransky N, et al. The cancer cell line encyclopedia enables predictive modelling of anticancer drug sensitivity. *Nature*. 2012;483:603-607.
17. Law MH, GenoMEL Consortium, Essen-Heidelberg Investigators, The SDH Study Group, Q-MEGA and QTWIN Investigators, AMFS Investigators, ATHENS Melanoma Study Group, et al. Genome-wide meta-analysis identifies five new susceptibility loci for cutaneous malignant melanoma. *Nat Genet*. 2015;47:987-995.
18. Visconti A, Duffy DL, Liu F, et al. Genome-wide association study in 176,678 Europeans reveals genetic loci for tanning response to sun exposure. *Nat Commun*. 2018;9:1684.

19. Landsberg J, Kohlmeyer J, Renn M, et al. Melanomas resist T-cell therapy through inflammation-induced reversible dedifferentiation. *Nature*. 2012;490:412-416.
20. Hoek KS, Eichhoff OM, Schlegel NC, et al. In vivo switching of human melanoma cells between proliferative and invasive states. *Cancer Res*. 2008;68:650-656.
21. Sauka-Spengler T, Bronner-Fraser M. A gene regulatory network orchestrates neural crest formation. *Nat Rev Mol Cell Biol*. 2008;9: 557-568.
22. Tsoi J, Robert L, Paraiso K, et al. Multi-stage differentiation defines melanoma subtypes with differential vulnerability to drug-induced iron-dependent oxidative stress. *Cancer Cell*. 2018;33:890-904.e5.
23. Verfaillie A, Imrichova H, Atak ZK, et al. Decoding the regulatory landscape of melanoma reveals TEADS as regulators of the invasive cell state. *Nat Commun*. 2015;6:6683.
24. Bessede A, Gargaro M, Pallotta MT, et al. Aryl hydrocarbon receptor control of a disease tolerance defence pathway. *Nature*. 2014;511: 184-190.
25. Vogel CFA, Khan EM, Leung PSC, et al. Cross-talk between aryl hydrocarbon receptor and the inflammatory response. *J Biol Chem*. 2014;289:1866-1875.
26. Stobbe-Maicherski N, Wolff S, Wolff C, et al. The interleukin-6-type cytokine oncostatin M induces aryl hydrocarbon receptor expression in a STAT3-dependent manner in human HepG2 hepatoma cells. *FEBS J*. 2013;280:6681-6690.
27. Stanford EA, Ramirez-Cardenas A, Wang Z, et al. Role for the aryl hydrocarbon receptor and diverse ligands in oral squamous cell carcinoma migration and tumorigenesis. *Mol Cancer Res*. 2016;14: 696-706.
28. Stanford EA, Wang Z, Novikov O, et al. The role of the aryl hydrocarbon receptor in the development of cells with the molecular and functional characteristics of cancer stem-like cells. *BMC Biol*. 2016; 14:20.
29. Diry M, Tomkiewicz C, Koehle C, et al. Activation of the dioxin/aryl hydrocarbon receptor (AhR) modulates cell plasticity through a JNK-dependent mechanism. *Oncogene*. 2006;25:5570-5574.
30. Yan B, Liu S, Shi Y, et al. Activation of AhR with nuclear IKKα regulates cancer stem-like properties in the occurrence of radioresistance. *Cell Death Dis*. 2018;9:1-15.
31. Fortes C, Mastroeni S, Melchi F, et al. The association between residential pesticide use and cutaneous melanoma. *Eur J Cancer*. 2007; 43:1066-1075.
32. Akhtar F, Garabrant D, Ketchum N, Michalek J. Cancer in US air force veterans of the Vietnam war. *J Occup Environ Med*. 2004;46:123-136.
33. Xue P, Fu J, Zhou Y. The Aryl Hydrocarbon Receptor and Tumor Immunity. *Front Immunol*. 2018;9: http://dx.doi.org/10.3389/fimmu.2018.00286.
34. Murray IA, Patterson AD, Perdew GH. Aryl hydrocarbon receptor ligands in cancer: friend and foe. *Nat Rev Cancer*. 2014;14: 801-814.
35. Brooks J, E. Eltom S. Malignant transformation of mammary epithelial cells by ectopic overexpression of the aryl hydrocarbon receptor. *CCDT* 2011;11:654–69.
36. Andersson P, McGuire J, Rubio C, et al. A constitutively active dioxin/aryl hydrocarbon receptor induces stomach tumors. *PNAS*. 2002; 99:9990-9995.
37. Moennikes O, Loeppen S, Buchmann A, et al. A constitutively active dioxin/aryl hydrocarbon receptor promotes hepatocarcinogenesis in mice. *Cancer Res*. 2004;64:4707-4710.
38. Pollet M, Shaik S, Mescher M, et al. The AHR represses nucleotide excision repair and apoptosis and contributes to UV-induced skin carcinogenesis. *Cell Death Differ*. 2018;25:1823-1836.
39. Ikuta T, Kawajiri K. Zinc finger transcription factor Slug is a novel target gene of aryl hydrocarbon receptor. *Exp Cell Res*. 2006;312:3585-3594.
40. Villano CM, Murphy KA, Akintobi A, White LA. 2,3,7,8-tetrachlorodibenzo-p-dioxin (TCDD) induces matrix metalloproteinase (MMP) expression and invasion in A2058 melanoma cells. *Toxicol Appl Pharmacol*. 2006;210:212-224.
41. Contador-Troca M, Alvarez-Barrientos A, Barrasa E, et al. The dioxin receptor has tumor suppressor activity in melanoma growth and metastasis. *Carcinogenesis*. 2013;34:2683-2693.
42. Corre S, Tardif N, Mouchet N, et al. Sustained activation of the aryl hydrocarbon receptor transcription factor promotes resistance to BRAF-inhibitors in melanoma. *Nat Commun*. 2018;9:4775.
43. Reiners JJ, Lee J-Y, Clift RE, Dudley DT, Myrand SP. PD98059 is an equipotent antagonist of the aryl hydrocarbon receptor and inhibitor of mitogen-activated protein kinase kinase. *Mol Pharmacol*. 1998;53: 438-445.
44. Opitz CA, Litzenburger UM, Sahm F, et al. An endogenous tumour-promoting ligand of the human aryl hydrocarbon receptor. *Nature*. 2011;478:197-203.
45. Mezrich JD, Fechner JH, Zhang X, Johnson BP, Burlingham WJ, Bradfield CA. An interaction between kynurenine and the aryl hydrocarbon receptor can generate regulatory T cells. *J Immunol*. 2010;185: 3190-3198.
46. Campesato LF, Budhu S, Tchaicha J, et al. Interaction between Kynurenine and the AhR is an effector mechanism of tumor immunosuppression and represents a potential immunotherapy target. *J Immunol*. 2018;200:177.5-177.5.
47. Nguyen NT, Kimura A, Nakahama T, et al. Aryl hydrocarbon receptor negatively regulates dendritic cell immunogenicity via a kynurenine-dependent mechanism. *PNAS*. 2010;107:19961-19966.
48. Labadie BW, Bao R, Luke JJ. Reimagining IDO pathway inhibition in cancer immunotherapy via downstream focus on the tryptophan–kynurenine–aryl hydrocarbon axis. *Clin Cancer Res*. 2019;25:1462-1471.
49. Liu Y, Lv J, Liu J, et al. STAT3/p53 pathway activation disrupts IFN-β–induced dormancy in tumor-repopulating cells. *J Clin Invest*. 2018; 128:1057-1073.
50. Munn DH, Sharma MD, Hou D, et al. Expression of indoleamine 2,3-dioxygenase by plasmacytoid dendritic cells in tumor-draining lymph nodes. *J Clin Invest*. 2004;114:280-290.

SUPPORTING INFORMATION

Additional supporting information may be found online in the Supporting Information section at the end of this article.

How to cite this article: Mengoni M, Braun AD, Gaffal E, Tüting T. The aryl hydrocarbon receptor promotes inflammation-induced dedifferentiation and systemic metastatic spread of melanoma cells. *Int. J. Cancer*. 2020;147: 2902–2913. https://doi.org/10.1002/ijc.33252